






# Ultrahigh Efficiency Four-Wave Mixing Wavelength Conversion in Packaged Silica Microrod Resonator

Daquan Yang , Yuanyuan Guo, Wen Chen, Yanran Wu, Kunpeng Zhai , Xin Wang, Jiabin Cui , Huashun Wen , and Chuan Wang , *Member, IEEE*

**Abstract**—Whispering-gallery-mode (WGM) resonator with high-quality factor ( $Q$ ) is a key platform for a wide range of fields including nonlinear optics, biosensing and quantum photonics. In this work, a packaged silica microrod resonator (PSMR) with ultrahigh- $Q$  of  $9.0 \times 10^8$  is experimentally demonstrated. Ultrahigh four-wave mixing conversion efficiency of  $-8.6$  dB at a pump power of 27 mW is achieved within this ultrahigh- $Q$  PSMR. Furthermore, this PSMR shows high stability of resonant wavelength shift within 0.032 pm. This work suggests that the PSMR may be a promising platform for optical signal processing and quantum photonics.

**Index Terms**—WGM resonator, packaged microrod, four-wave mixing, wavelength conversion, conversion efficiency.

## I. INTRODUCTION

**F**OUR-WAVE mixing (FWM) is an essential nonlinear effect based on Kerr optical nonlinearity for a broad range of

applications such as wavelength conversion, parametric oscillation, and optical frequency comb generation [1], [2], [3], [4]. In recent years, wavelength conversion based on FWM effect has been demonstrated in various platforms, such as semiconductor optical amplifiers [5], [6], [7], optical waveguides [8], [9], [10], [11], [12], [13], highly nonlinear fibers [14], [15], optical microcavities including photonics crystal microcavities [16] and whispering-gallery-mode (WGM) resonators [17], [18], [19] and so on. Particularly, WGM resonators [20] with high-quality factor ( $Q$ ) enable strong light confinement, making them excellent candidates for improving the FWM efficiency [21], [22], [23], [24], [25], [26], [27], [28]. X. Hu et al. demonstrated a FWM-based wavelength conversion in graphene-silicon microring resonator, and the FWM conversion efficiency (CE) of  $-38$  dB was obtained when the pump power was 20 mW [23]. E. Stassen et al. demonstrated an aluminum gallium arsenide on-insulator microring resonator with a  $Q \sim 10^5$  and FWM CE of  $-16$  dB at the pump power of 32 mW [26]. P. Xing et al. demonstrated an amorphous silicon carbide ring resonator with  $Q$  of 70,000 and FWM CE of  $-21$  dB when the pump power was 15 mW [27]. Moreover, a titanium dioxide microring resonator with a  $Q$  of  $1.4 \times 10^5$  and FWM CE of  $-31$  dB at a pump power of 40 mW was demonstrated by M. Fu et al. [28]. However, FWM CE of the WGM resonators mentioned above is limited around  $-40 \sim -16$  dB, owing to the low power intensity inside the resonators caused by the limited  $Q$  ( $\sim 10^5$ ).

In this paper, highly efficient FWM-based wavelength conversion is achieved in a packaged silica microrod resonator (PSMR) with ultrahigh- $Q \sim 9.0 \times 10^8$ . The FWM CE of  $-8.6$  dB is achieved when the pump power is 27 mW due to the high optical confinement. Additionally, compared with the fabrication of these typical on-chip resonators, the silica microrod resonator is fabricated using an automatical laser-machine reflow process, which supports resonator fabrication at a fast and cost-effective rate. Moreover, by introducing packaging technology for the microrod resonators, a drastic improvement of coupling stability is realized to alleviate environmental perturbations. Furthermore, the PSMR exhibits the superior long-term stability achieved by fine temperature adjustment via a thermoelectric cooler (TEC). The demonstration of the highly efficient wavelength conversion in the PSMR suggests that the performance of the high energy-efficient optical signal processing, such as wavelength conversion and optical frequency comb generation may be improved by the utilization of this PSMR.

Manuscript received 2 August 2022; revised 28 September 2022 and 14 November 2022; accepted 1 December 2022. Date of publication 15 December 2022; date of current version 16 March 2023. This work was supported in part by the National Key R&D Program of China under Grants 2020YFB2205801 and 2019YFB2203104, in part by the National Natural Science Foundation of China under Grants 11974058 and 62131002, in part by the Beijing Nova Program through Beijing Municipal Science and Technology Commission under Grant Z201100006820125, in part by the Beijing Natural Science Foundation under Grant Z210004, in part by the State Key Laboratory of Information Photonics and Optical Communications under Grant IPOC2021ZT01 BUPT, China, and in part by the Fundamental Research Funds for the Central Universities under Grant 2022RC02. (Corresponding author: Huashun Wen; Chuan Wang.)

Daquan Yang is with the State Key Laboratory of Information Photonics and Optical Communications, Beijing University of Posts and Telecommunications, Beijing 100876, China, and with the School of Information and Communication Engineering, Beijing University of Posts and Telecommunications, Beijing 100876, China, and also with the School of Information Science and Technology, Tibet University, Lhasa 850000, China (e-mail: ydq@bupt.edu.cn).

Yuanyuan Guo, Wen Chen, Yanran Wu, and Jiabin Cui are with the State Key Laboratory of Information Photonics and Optical Communications, Beijing University of Posts and Telecommunications, Beijing 100876, China (e-mail: guoyy@bupt.edu.cn; chenwen0103@bupt.edu.cn; wuyanran@bupt.edu.cn; cuijiabin@bupt.edu.cn).

Kunpeng Zhai, Xin Wang, and Huashun Wen are with the State Key Laboratory on Integrated Optoelectronics, Institute of Semiconductors, Chinese Academy of Sciences, Beijing 100083, China, and also with the School of Electronic, Electrical and Communication Engineering, University of Chinese Academy of Sciences, Beijing 100049, China (e-mail: kpzhai@semi.ac.cn; wxin@semi.ac.cn; whs@semi.ac.cn).

Chuan Wang is with the School of Artificial Intelligence, Beijing Normal University, Beijing 100875, China (e-mail: wangchuan@bnu.edu.cn).

Color versions of one or more figures in this article are available at <https://doi.org/10.1109/JLT.2022.3226724>.

Digital Object Identifier 10.1109/JLT.2022.3226724

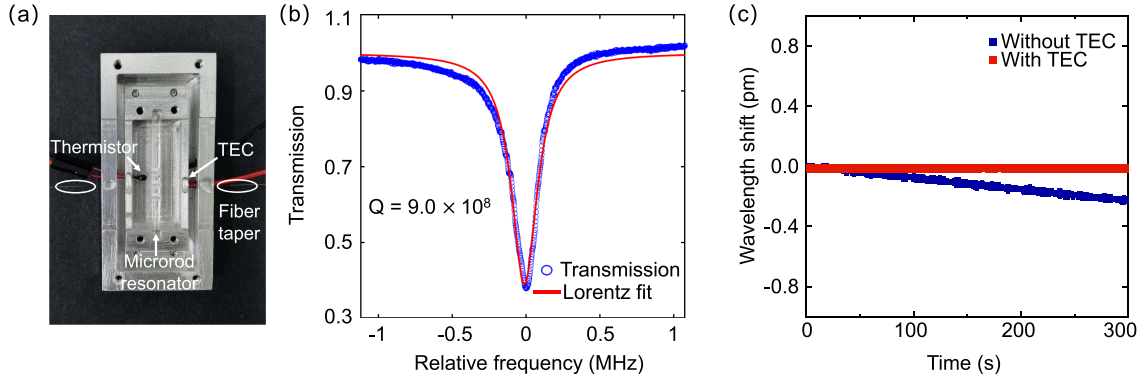


Fig. 1. (a) Photograph of the PSMR, consisting of a silica microrod resonator with diameter of 3.0 mm, a coupling fiber taper, a TEC and a thermistor. (b) Measured and fitted transmission spectra the PSMR. (c) The stability of the resonant wavelength in the PSMR without TEC (blue line) and with TEC (red line). TEC, thermoelectric cooler.

## II. FABRICATION AND CHARACTERIZATION OF THE PSMR

The PSMR basically consists of three major building blocks: a silica microrod resonator with diameter of 3.0 mm, a coupling fiber taper, a TEC and a thermistor. Fig. 1(a) depicts the photograph of the PSMR in which the microrod resonator is automatically fabricated with the laser-machine reflow process. This automatic fabrication process provides a highly repeatable, reliable, fast and cost-effective method for microcavity fabrication. The measured transmission spectrum (the blue dotted line) of the fundamental TE mode at wavelength around 1560 nm is plotted in Fig. 1(b). The transmission spectrum is fitted by a Lorentz curve, as shown by the red line in Fig. 1(b). Therefore, an ultrahigh- $Q$  ( $Q_L$ ) of  $9.0 \times 10^8$  is obtained. The  $Q_L$  in the PSMR can be expressed by [29]

$$Q_L^{-1} = Q_{in}^{-1} + Q_c^{-1} \quad (1)$$

where the intrinsic  $Q$  ( $Q_{in}$ ) is  $1.1 \times 10^9$ . The coupling  $Q$  ( $Q_c$ ) can be derived with a value of  $4.9 \times 10^9$ . Furthermore, we characterize the stability of the resonant wavelength by monitoring the real-time wavelength shift of the PSMR with and without TEC, as depicted in Fig. 1(c). The resonant mode of the microrod resonator is sensitive to cavity temperature and it will shift because of the thermo-optic effect caused by the large injection power and ambient temperature fluctuations. To alleviate this situation, a TEC is used to stabilize the temperature of the PSMR. The TEC maintains the PSMR temperature stable through the feedback monitored by the thermistor. The resonant wavelength shifts about 0.2 pm in the short-wave direction under the condition of without TEC. The wavelength shift may be caused by environmental temperature fluctuation and the laser wavelength self-drifting. With the control of a TEC, the maximum wavelength shift is 0.032 pm, which is 0.168 pm smaller than that without TEC. Note that the resonant mode remains a very stable state up to 300 seconds, as shown by the blue line in Fig. 1(c). Since the resonant mode is stabilized, the PSMR platform exhibits high robustness, stability, and portability. Benefitting from these advantages of the PSMR platform, the performance of FWM-based wavelength conversion could be improved.

## III. WORKING PRINCIPLE AND EXPERIMENTAL SETUP

Silica exhibits a large nonlinear coefficient  $\chi^{(3)}$  ( $n_2 = 3.2 \times 10^{-16} \text{ cm}^2/\text{W}$ ), which contributes to the strong nonlinearity [30]. Since  $\chi^{(3)}$  relates with third-order nonlinear processes, a FWM effect is demonstrated in the PSMR, as illustrated in Fig. 2(a) and (b). The FWM effect is the annihilation of photons from one or more waves and the creation of new photons at different frequencies. When the phase matching condition is satisfied, a strong FWM effect will occur. A pump light wave ( $p_1$ ) and the signal light wave ( $s_1$ ) are coupled into the PSMR, and two newly converted idler light waves ( $i_1$  and  $i_2$ ) are generated at lower and higher frequencies through the FWM effect [31]. The frequencies of pump light, signal light and two idler lights are respectively described as  $\omega_{(p_1)}$ ,  $\omega_{(s_1)}$ ,  $\omega_{(i_1)}$  and  $\omega_{(i_2)}$ . The frequencies of the two newly generated lights can be defined as  $\omega_{(i_1)} = \omega_{(p_1)} + \omega_{(s_1)} - \omega_{(i_2)}$ ,  $\omega_{(i_2)} = \omega_{(p_1)} + \omega_{(s_1)} - \omega_{(i_1)}$ , respectively. Depending on the frequencies of the pump light and signal light, the FWM effect can be divided into degenerate and non-degenerate processes. In this paper, the dispersion of the operating mode is anomalous, and the optical parametric oscillation process based on degenerate FWM could be easily occurred due to the well-matched phase-matching. The wavelength conversion based on the degenerate FWM effect is mainly considered and analyzed.

Fig. 2(c) depicts an illustration of the experimental setup of wavelength conversion based on FWM effect in the PSMR. Two individual continuous-wave lasers, which are defined as pump and signal light respectively, are generated by tunable lasers (TLs). The arbitrary function generator is used to send an electrical signal to the piezoelectric transducer inside the TL for fine tuning the laser frequency. Then the two lights are amplified by Erbium-doped fiber amplifiers (EDFAs) and their polarization are adjusted by fiber polarization controllers (PCs), respectively. The pump and signal lights are combined by a 50:50 coupler and coupled into the PSMR by a fiber taper. The transmission spectrum of the PSMR is detected by a low-noise photodetector while the FWM optical spectra are analyzed by an optical spectrum analyzer (OSA). The optical powers of the input lights are measured by a power meter and a 99:1 coupler.

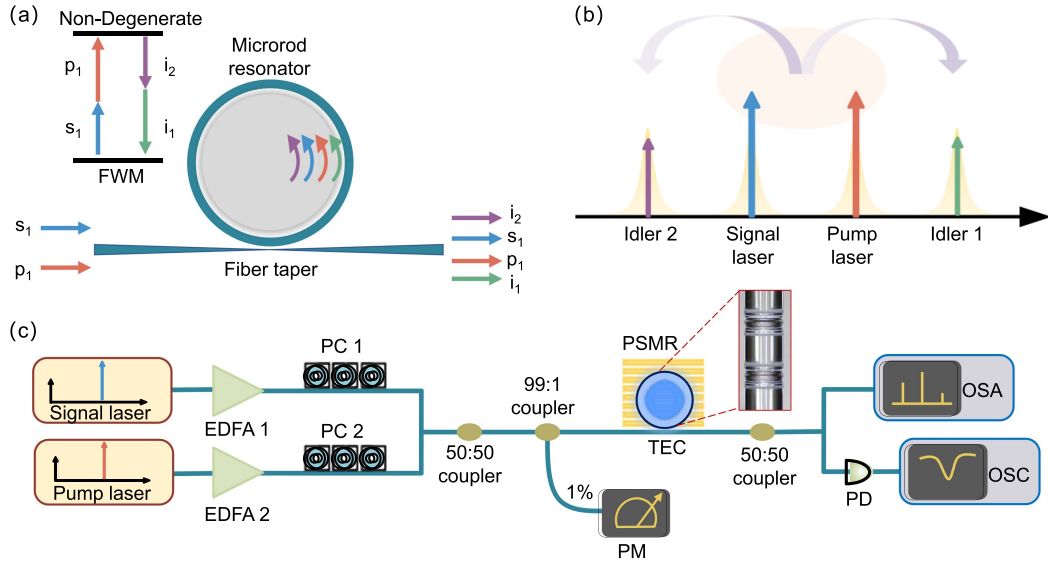


Fig. 2. (a) Schematic diagram of the principle of the FWM effect in the PSMR. (b) Illustration of the optical spectrum of the FWM effect. (c) Experimental setup of wavelength conversion based on FWM effect in the PSMR. Inset: the microscope image of the silica microrod resonator with diameter of 3.0 mm. EDFA, Erbium-doped fiber amplifier; PC, polarization controller; PSMR, packaged silica microrod resonator; TEC, thermoelectric cooler; PM, power meter; PD, photodetector; OSA, optical spectrum analyzer; OSC, oscilloscope.

A TEC and a thermistor is used to control and monitor the temperature of the PSMR platform.

#### IV. EXPERIMENTAL RESULTS

To characterize the performance of FWM-based wavelength conversion in the PSMR, we first measure the FWM effect with a low-power signal. Under the condition of low-power signal, the signal power is  $3.43 \mu\text{W}$ , which is at the minimum state to realize FWM wavelength conversion. With a signal light and a pump light coupling into the PSMR, the wavelength conversion is achieved, as illustrated in Fig. 3(a). The signal and pump waves are fine-tuned at the wavelengths of 1555.556 nm and 1557.596 nm, and an idler can be clearly observed at the wavelength of 1559.660 nm when the PSMR is on-resonance. By measuring the optical spectrum output from the PSMR, the CEs as a function of different input pump powers are plotted in Fig. 3(b). Here, the CE is defined as the ratio of converted idler power to the signal power [19], [22], [27]. The dependence of CE on pump power is measured from the output spectra from the PSMR. It can be observed that the CE linearly rises as the growth of the pump power. The maximum FWM CE of  $-5.46 \text{ dB}$  is obtained at pump power of 21.0 mW. In addition, the CE is determined by the field enhancement factor ( $FE$ ), which can be represented in the following form [28], [32]:

$$FE^2 = \frac{FSR}{\pi \cdot \Delta f_{FWHM}} \frac{2Q_L}{Q_c} \quad (2)$$

where  $FE^2$  is the power enhancement factor,  $FSR$  is the free spectral range of the resonator,  $\Delta f_{FWHM}$  is the PSMR's linewidth of the resonance, respectively. The field enhancement factor ( $FE$ ) is calculated to be  $\sim 157$ .

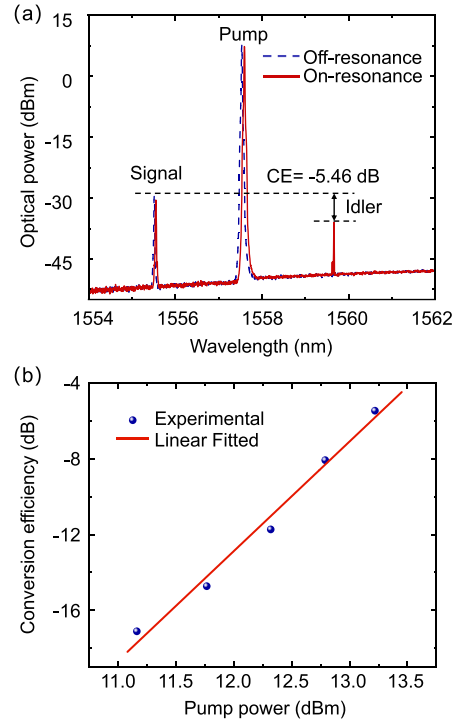


Fig. 3. Wavelength conversion measurements based on FWM with a low-power signal. (a) Measured FWM spectra output from the PSMR. (b) Measured CE versus the input pump power.

Although the FWM CE is obtained at the maximum of  $-5.46 \text{ dB}$  under a low-power signal, we find that the FWM process cannot stay stable resonance long enough for subsequent signal processing. It may be caused by the thermal fluctuations in the microrod cavity. Therefore, we propose a high-power signal

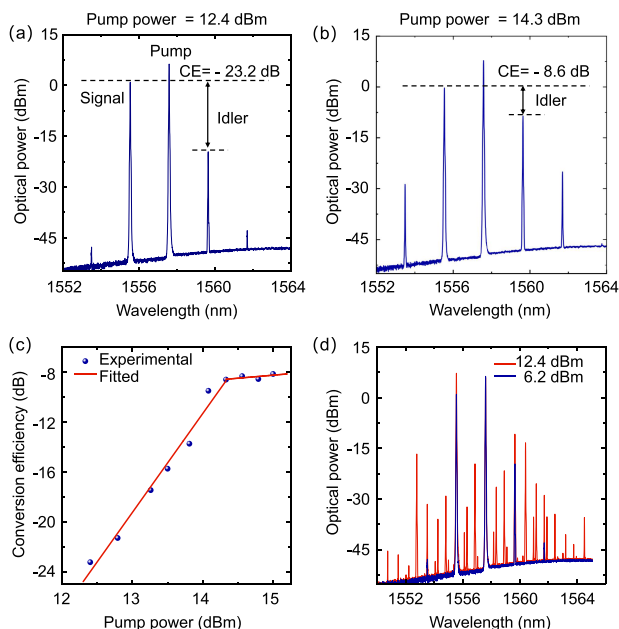


Fig. 4. Wavelength conversion measurements based on FWM with a high-power signal. (a) Measured FWM spectra output from the PSMR when the pump power is 17.4 mW (12.4 dBm). (b) Measured FWM spectra output from the PSMR when pump power is increased to 27.0 mW (14.3 dBm). (c) Measured CE versus the input pump power. (d) Cascaded FWM spectra of the PSMR when the power of signal light is change from 4.1 mW (6.2 dBm) to 17.2 mW (12.4 dBm).

FWM experiment at the same wavelength by increasing the power of signal to mW level to simultaneously maintain high signal quality and long-term stability.

The typical output spectra when the signal power is increased from 3.43  $\mu$ W to 4.2 mW with the pump power of 17.4 mW (12.4 dBm) are depicted in Fig. 4(a). The wavelengths of signal light, pump light and idler light are read out from OSA at 1555.540 nm, 1557.588 nm and 1559.648 nm, respectively. We can ignore the differences in wavelengths between the weak and strong signal schemes due to the OSA limited resolution of 0.02 nm. The corresponding CE of  $-23.2$  dB is obtained under this condition. The FWM CE is improved to  $-8.6$  dB when the power of pump is increased to 27.0 mW (14.3 dBm), as illustrated in Fig. 4(b). Fig. 4(c) depicts the CEs as a function of different input pump powers while the signal power is fixed. The CE linearly increase as the power of pump is increased to 27.0 mW. The CE does not increase when the pump power exceeds 27.0 mW. Since the PSMR enhances the circulation of light, the maximum CE is obtained with the minimized power penalty. While the power of the pump is high, the instability caused by the thermo-optic effect appears in the cavity. As a result, the three wavelengths cannot completely stay in the resonance state, and the CE is close to the saturation state with the pump power.

We change the power of signal light from 4.1 mW to 17.2 mW and then measure the spectra of FWM effect. For the case of signal power with power of 4.1 mW, the first-order idlers are obtained as the blue line shows in Fig. 4(d). The cascaded FWM effect is achieved by reducing the amount of the detuning of pump light and signal light. Furthermore, multiple wavelength components are generated by the interaction with the

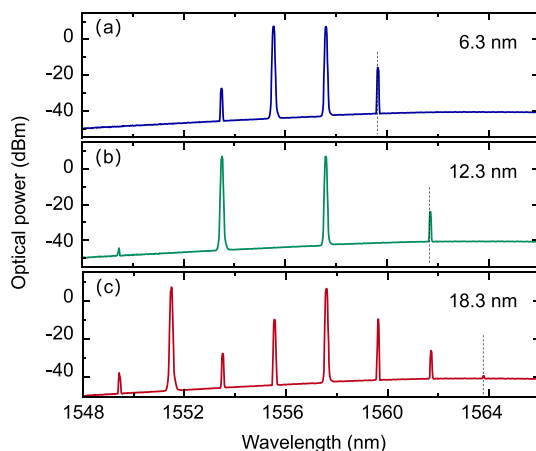


Fig. 5. Measurement of the FWM bandwidth with a high-power signal. The bandwidth of the output spectra is (a) 6.3 nm, (b) 12.3 nm and (c) 18.3 nm when the pump light is fixed at 1557.576 nm and the signal light is tuned at 1555.536 nm, 1553.516 nm and 1551.476 nm, respectively.

concomitant beams. The spectrum becomes dense and finally the optical frequency comb is generated. The optical frequency comb generated in the PSMR has potential applications in the fields of precision spectroscopy, soliton transmission and optical communication.

Fig. 5 depicts the wavelength conversion range under the high-power signal scheme. The wavelength of signal light is finely tuned while the pump light is fixed at 1557.576 nm. The wavelength of the signal light is tuned at 1555.536 nm, 1553.516 nm and 1551.476 nm, resulting in a broad bandwidth of 6.3 nm, 12.3 nm and 18.3 nm, respectively. The power of the idler light shown in Fig. 5(c) may not sufficient for signal analysis. This may be due to the fact that the pump and the signal light interact with each concomitant beams to generate additional idlers, so that part of the energy is transferred to the sideband idlers. With the improvement of fabrications, the bandwidth might be increased and the PSMR will achieve highly efficient wavelength conversion over broad bandwidths. Moreover, the PSMR can be tuned by the thermo-optic effect. The PSMR can be precisely controlled by the TEC to measure the thermal characteristics, as illustrated in the Fig. 6. The resonant wavelength increases linearly when the temperature increases from 25.1  $^{\circ}$ C to 33.1  $^{\circ}$ C. According to the linear fitting depicted in Fig. 6(a), we obtain the resonant wavelength shift via the thermo-optic effect,  $d\lambda/dT = 7.08$  pm/K for the PSMR [33]. Fig. 6(b) depicts the output FWM spectra under different temperature conditions, which shows the tunability of the wavelength conversion in the PSMR. The tunability of wavelength conversion in the PSMR is characterized by precisely controlling the mode shift via the thermo-optic effect.

Fig. 7 shows the performance of different FWM-based wavelength conversion in WGM resonators. An improvement of CE is mainly dependent on ultrahigh- $Q$  factors caused by the low cavity loss of the PSMR. The limited  $Q$  leads to more power penalty and the CE is also restricted by the power consumption. Table I summarizes FWM wavelength conversion performances, including the nonlinear refractive index  $n_2$ , the

TABLE I  
FWM-BASED WAVELENGTH CONVERSION PERFORMANCE COMPARISON FOR DIFFERENT NONLINEAR MATERIALS

Nonlinear material	Platform	$n_2$ (m <sup>2</sup> /W)	Field enhancement factor (FE)	Quality factor ( $Q$ )	Pump power (mW)	Conversion efficiency (dB)	Publication year	Reference
Si <sub>7</sub> N <sub>3</sub>	Waveguide	$2.8 \times 10^{-17}$	–	–	23.4	-24.9	2017	[11]
Si <sub>3</sub> N <sub>4</sub>	Waveguide	$2.5 \times 10^{-19}$	–	–	2138.0	-26.1	2015	[12]
Si <sub>x</sub> N <sub>y</sub>	Waveguide	$1.6 \times 10^{-18}$	–	–	320	-30	2017	[13]
Silicon	Microring	$6.5 \times 10^{-18}$	–	19,000	11.3	-25.4	2008	[21]
Hydex	Microring	$1.2 \times 10^{-19}$	17.9	$1.2 \times 10^6$	8.8	-36	2009	[22]
Si/Graphene	Microring	–	–	–	22.4	-38	2011	[23]
Ta <sub>2</sub> O <sub>5</sub>	Microring	$1.4 \times 10^{-18}$	50	$1.8 \times 10^5$	6	-30	2017	[24]
AlGaAs	Microring	$2.6 \times 10^{-17}$	11	44,000	7	-12	2018	[25]
SiC	Microring	$4.8 \times 10^{-18}$	6.3	70,000	15	-21	2020	[27]
TiO <sub>2</sub>	Microring	$2.5 \times 10^{-19}$	3.9	$1.4 \times 10^5$	45.7	-32.4	2020	[28]
Silicon	<sup>a</sup> CROW	$6.5 \times 10^{-18}$	–	–	15.8	-36	2011	[17]
Silica	Microrod	$3.2 \times 10^{-20}$	157	$9 \times 10^8$	27	-8.6	2022	This work

<sup>a</sup>CROW is the abbreviation for coupled-resonator optical waveguide.

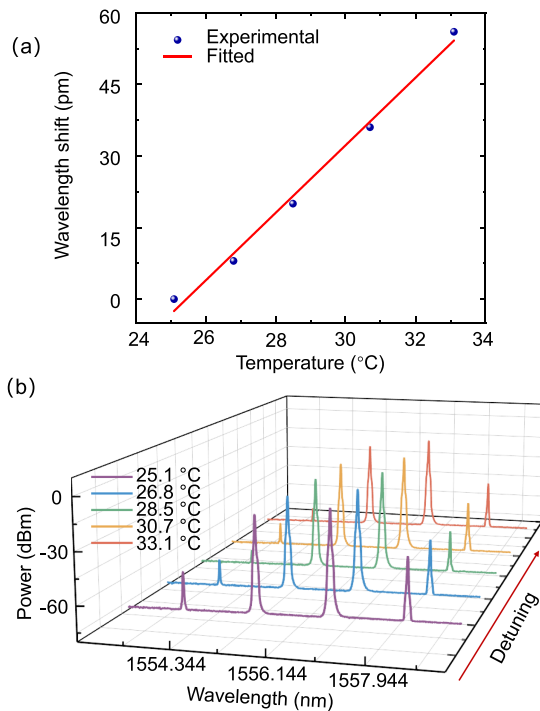


Fig. 6. (a) Measured resonant wavelength shift of the PSMR versus temperature. (b) The output FWM spectra when the PSMR is tuned by the thermo-optic effect.

field enhancement factor (FE), and the quality factor ( $Q$ ), for different resonators and materials. Most of the demonstrated CEs are below  $-20$  dB. In our work, by introducing lathe machining and packaging technology to the fabrication of the microrod resonators, the ultrahigh- $Q$  factors are maintained to allow the cavity enhancement with their capability to recycle the pump power. The highly efficient wavelength conversion realized by the PSMR illuminates the promising prospects in optical signal processing domain such as wavelength converters.

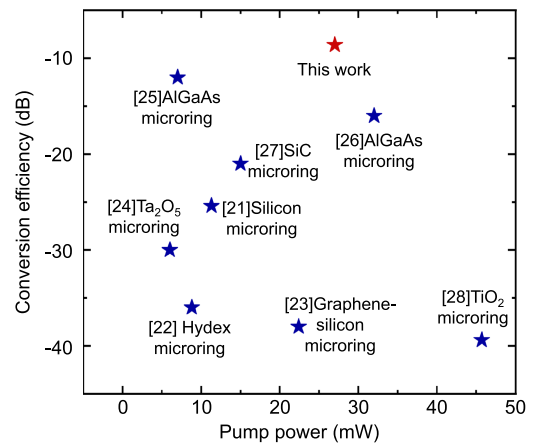


Fig. 7. FWM-based wavelength conversion performance comparison for different WGM resonators. Horizontal axis is pump power while vertical axis is the CE.

## V. CONCLUSION

In summary, we fabricate a PSMR with an ultrahigh- $Q$  and evaluate the performance of the device via the FWM-based wavelength conversion experiments. First, we fabricate the microrod resonator using the lathe machined technology and package the resonator. The PSMR exhibits the ultrahigh- $Q$  and maintains the superior long-term stability due to the packaging technology and the utilization of the TEC. The highly efficient wavelength conversion through FWM process is reported by evaluating the performance of the PSMR under different pump power, signal power and wavelength. The CE of  $-5.46$  dB is obtained with the pump power of 21.0 mW and low-power signal of  $3.43 \mu\text{W}$ , and the comparable CE of  $-8.6$  dB is achieved under the condition of pump power at 27.0 mW and high-power signal at 4.1 mW. The resonant wavelength shift of the PSMR via the thermo-optic effect is obtained as 7.08 pm/K. The bandwidth of the wavelength conversion is measured up

to 18.3 nm. These achievements strongly support the PSMR with the ability of highly effective nonlinearity and low energy consumption. It is anticipated that the ultrahigh- $Q$  PSMR might satisfy more interesting demand for achieving optical signal processing and quantum photonics functions.

#### ACKNOWLEDGMENT

The authors would like to thank Prof. Cheng Wang from City University of Hong Kong and Dr. Qitao Cao from PeKing University for helpful discussions.

#### REFERENCES

- [1] J. Leuthold, C. Koos, and W. Freude, "Nonlinear silicon photonics," *Nature Photon.*, vol. 4, no. 8, pp. 535–544, 2010.
- [2] L. Razzari et al., "CMOS-compatible integrated optical hyper-parametric oscillator," *Nature Photon.*, vol. 4, no. 1, pp. 41–45, 2010.
- [3] T. J. Kippenberg, R. Holzwarth, and S. A. Diddams, "Microresonator-based optical frequency combs," *Science*, vol. 332, no. 6029, pp. 555–559, 2011.
- [4] Y. Yang et al., "Graphene-enhanced polarization-insensitive all-optical wavelength conversion based on four-wave mixing," *Opt. Exp.*, vol. 30, no. 6, pp. 10168–10177, 2022.
- [5] B. Filion, L. Jiachuan, A. T. Nguyen, X. Zhang, S. LaRochelle, and L. A. Rusch, "Semiconductor optical amplifier-based wavelength conversion of nyquist-16QAM for flex-grid optical networks," *J. Lightw. Technol.*, vol. 34, no. 11, pp. 2724–2729, 2016.
- [6] T. Ohtsuki and M. Matsuura, "Wavelength conversion of 25-Gbit/s PAM-4 signals using a quantum-dot SOA," *IEEE Photon. Technol. Lett.*, vol. 30, no. 5, pp. 459–462, Mar. 2018.
- [7] A. A. E. Hajomer et al., "On-chip all-optical wavelength conversion of PAM-4 signals using an integrated SOA-based turbo-switch circuit," *J. Lightw. Technol.*, vol. 37, no. 16, pp. 3956–3962, Aug. 2019.
- [8] C. Wang et al., "Ultrahigh-efficiency wavelength conversion in nanophotonic periodically poled lithium niobate waveguides," *Optica*, vol. 5, no. 11, pp. 1438–1441, 2018.
- [9] D. Grassani, M. H. Pfeiffer, T. J. Kippenberg, and C.-S. Brès, "Second- and third-order nonlinear wavelength conversion in an all-optically poled Si<sub>3</sub>N<sub>4</sub> waveguide," *Opt. Lett.*, vol. 44, no. 1, pp. 106–109, 2019.
- [10] P. Che, K. Baumgaertl, A. Kúkol'ová, C. Dubs, and D. Grundler, "Efficient wavelength conversion of exchange magnons below 100 nm by magnetic coplanar waveguides," *Nature Commun.*, vol. 11, no. 1, pp. 1–9, 2020.
- [11] K. Ooi et al., "Pushing the limits of CMOS optical parametric amplifiers with USRN: Si<sub>7</sub>N<sub>3</sub> above the two-photon absorption edge," *Nature Commun.*, vol. 8, no. 1, pp. 1–10, 2017.
- [12] C. J. Krüchel et al., "Continuous wave-pumped wavelength conversion in low-loss silicon nitride waveguides," *Opt. Lett.*, vol. 40, no. 6, pp. 875–878, 2015.
- [13] C. Lacava et al., "Si-rich silicon nitride for nonlinear signal processing applications," *Sci. Rep.*, vol. 7, no. 1, pp. 1–13, 2017.
- [14] G.-W. Lu, T. Sakamoto, and T. Kawanishi, "Wavelength conversion of optical 64QAM through FWM in HNLF and its performance optimization by constellation monitoring," *Opt. Exp.*, vol. 22, no. 1, pp. 15–22, 2014.
- [15] S. Singh, S. Singh, Q. M. Ngo, and A. M. Mohammadi, "Analysis of all-optical wavelength converter based on FWM effect in HNLF for coherent 100 Gbps dual-polarized DQPSK signal," *Opt. Fiber Technol.*, vol. 59, 2020, Art. no. 102323.
- [16] G. Marty, S. Combríe, F. Raineri, and A. D. Rossi, "Photonic crystal optical parametric oscillator," *Nature Photon.*, vol. 15, no. 1, pp. 53–58, 2021.
- [17] F. Morichetti, A. Canciamilla, C. Ferrari, A. Samarelli, M. Sorel, and A. Melloni, "Travelling-wave resonant four-wave mixing breaks the limits of cavity-enhanced all-optical wavelength conversion," *Nature Commun.*, vol. 2, no. 1, pp. 1–8, 2011.
- [18] M. Yu et al., "Raman lasing and soliton mode-locking in lithium niobate microresonators," *Light Sci. Appl.*, vol. 9, no. 1, pp. 1–7, 2020.
- [19] W. C. Jiang, K. Li, X. Gai, D. A. Nolan, and P. Dainese, "Ultra-low-power four-wave mixing wavelength conversion in high- $Q$  chalcogenide microring resonators," *Opt. Lett.*, vol. 46, no. 12, pp. 2912–2915, 2021.
- [20] K. J. Vahala, "Optical microcavities," *Nature*, vol. 424, no. 6950, pp. 839–846, 2003.
- [21] A. C. Turner, M. A. Foster, A. L. Gaeta, and M. Lipson, "Ultra-low power parametric frequency conversion in a silicon microring resonator," *Opt. Exp.*, vol. 16, no. 7, pp. 4881–4887, 2008.
- [22] M. Ferrera et al., "Low power four wave mixing in an integrated, micro-ring resonator with  $Q = 1.2$  million," *Opt. Exp.*, vol. 17, no. 16, pp. 14098–14103, 2009.
- [23] X. Hu et al., "Graphene-silicon microring resonator enhanced all-optical up and down wavelength conversion of QPSK signal," *Opt. Exp.*, vol. 24, no. 7, pp. 7168–7177, 2016.
- [24] C.-L. Wu et al., "Efficient wavelength conversion with low operation power in a Ta<sub>2</sub>O<sub>5</sub>-based micro-ring resonator," *Opt. Lett.*, vol. 42, no. 23, pp. 4804–4807, 2017.
- [25] M. Pu et al., "Ultra-efficient and broadband nonlinear AlGaAs-on-insulator chip for low-power optical signal processing," *Laser Photon. Rev.*, vol. 12, no. 12, 2018, Art. no. 1800111.
- [26] E. Stassen et al., "Ultra-low power all-optical wavelength conversion of high-speed data signals in high-confinement AlGaAs-on-insulator microresonators," *APL Photon.*, vol. 4, no. 10, 2019, Art. no. 100804.
- [27] P. Xing, D. Ma, L. C. Kimerling, A. M. Agarwal, and D. T. Tan, "High efficiency four wave mixing and optical bistability in amorphous silicon carbide ring resonators," *APL Photon.*, vol. 5, no. 7, 2020, Art. no. 076110.
- [28] M. Fu et al., "High- $Q$  titanium dioxide micro-ring resonators for integrated nonlinear photonics," *Opt. Exp.*, vol. 28, no. 26, pp. 39084–39092, 2020.
- [29] M. L. Gorodetsky and V. S. Ilchenko, "Optical microsphere resonators: Optimal coupling to high- $Q$  whispering-gallery modes," *J. Opt. Soc. Amer. B*, vol. 16, no. 1, pp. 147–154, 1999.
- [30] B. J. Eggleton, B. Luther-Davies, and K. Richardson, "Chalcogenide photonics," *Nature Photon.*, vol. 5, no. 3, pp. 141–148, 2011.
- [31] J. Lu, T. Liu, Y. Wang, J. Liu, and J. He, "Research on polarization insensitive AOWC system for 40 Gbps 16QAM-OFDM based on wide optical comb generation self-pumping structure," *Opt. Fiber Technol.*, vol. 65, 2021, Art. no. 102611.
- [32] M. Soltani, "Novel integrated silicon nanophotonic structures using ultrahigh  $q$  resonators," Ph.D. dissertation, Georgia Inst. Technol., Atlanta, GA, USA, 2009.
- [33] D. Yang et al., "Packaged microbubble resonator for versatile optical sensing," *J. Lightw. Technol.*, vol. 38, no. 16, pp. 4555–4559, 2020.

**Daquan Yang** received the B.S. degrees in electronic information science and technology from the University of Jinan, Jinan, China, in 2005, the Ph.D. degree in information and communication engineering from the Beijing University of Posts and Telecommunications, Beijing, China, in 2014. From 2012 to 2014, he was a Visiting Fellow with Harvard University, Cambridge, MA, USA. He is currently a Professor with the Beijing University of Posts and Telecommunications. His research interests include high-sensitivity optical sensing and high-speed optical communication.

**Yuanyuan Guo** received the B.S. degree in information and communication engineering in 2020 from the Beijing University of Posts and Telecommunications, Beijing, China, where she is currently working toward the master's degree in biomedical engineering. Her research focuses on microcavity nonlinearity and applications.

**Wen Chen** received the B.S. degree in electronic information engineering from Shandong Normal University, Jinan, China, in 2016. She is currently working toward the master's degree in information and communication engineering with the Beijing University of Posts and Telecommunications, Beijing, China. Her research focuses on optical frequency comb.

**Yanran Wu** received the B.S. degree in communication engineering from Shandong Normal University, Jinan, China, in 2016, and the master's degree in electronics and communication engineering from the University of International Relations, Beijing, China, in 2020. She is currently working toward the Ph.D. degree in information and communication engineering with the Beijing University of Posts and Telecommunications, Beijing. Her research focuses on microwave photonic sensing.

**Kunpeng Zhai** is currently working toward the Ph.D. degree with the Institute of Semiconductor, Chinese Academy of Sciences, Beijing, China. His research interests include microwave photonics and silicon photonics.

**Xin Wang** is currently an Associate Professor with the Institute of Semiconductor, Chinese Academy of Sciences, Beijing, China. His research interests include microwave photonics and silicon photonics.

**Jiabin Cui** received the Ph.D. degree from the State Key Laboratory of Information Photonics and Optical Communications, Beijing University of Posts and Telecommunications (BUPT), Beijing, China, in 2019. He is currently a Lecturer with the School of Information and Communication Engineering, BUPT. His research interests include optical signal processing, advanced optical modulation, and optical parametric amplifiers.

**Huashun Wen** is currently an Associate Professor with the Institute of Semiconductor, Chinese Academy of Sciences, Beijing, China. His research interests include microwave photonics and silicon photonics.

**Chuan Wang** (Member, IEEE) received the B.S. degree in physics from Shandong University, Jinan, China, in 2003, and the Ph.D. degree in physics from Tsinghua University, Beijing, China, in 2008. He is currently a Professor with the Beijing Normal University, Beijing. His research interests include microcavity photonics and quantum communication.